Surfactants and polymers on nanoscale surfaces: the interface landscape of plasmonic nanostars

frontiers | Frontiers in Nanotechnology

TYPE Mini Review
PUBLISHED 24 December 2024
DOI 10.3389/fnano.2024.1505304

OPEN ACCESS

EDITED BY
Giulio Fracasso,
University of Padova, Italy

REVIEWED BY
Subina Raveendran,
Tandem PV, Inc., United States

*CORRESPONDENCE
Laura Fabris,
laura.fabris@polito.it

RECEIVED 02 October 2024
ACCEPTED 05 December 2024
PUBLISHED 24 December 2024

CITATION
Ferrari D, Deriu C and Fabris L (2024) Surfactants and polymers on nanoscale surfaces: the interface landscape of plasmonic nanostars. *Front. Nanotechnol.* 6:1505304. doi: 10.3389/fnano.2024.1505304

Surfactants and polymers on nanoscale surfaces: the interface landscape of plasmonic nanostars

Debora Ferrari, Chiara Deriu and Laura Fabris*

Department of Applied Science and Technology, Politecnico di Torino, Torino, Italy

Surfactants and polymers are widely used as shape-directing agents in the synthesis of colloidal plasmonic nanostars, consequently acting as non-negligible players in all those high-performance applications in which processes occur at their interfaces, such as surface enhanced Raman spectroscopy (SERS) and plasmon-induced catalysis. Therefore, elucidating surfactant- and polymer-metal interactions is critical to rationally improving the performance of nanostars in the same range of applications. In this mini-review, we present traditional and state-of-the-art characterization methods that can be used to investigate the ligand-surface interactions that occur on mature nanostars. Due to historically based limitations in the availability of nanostar-specific literature, we utilize nanorod literature as a starting point to critically infer which analytical approaches can be seamlessly translated to nanostar systems, and which instead need to be adapted to intercept the peculiar needs imposed by the branched nanoparticle morphology.

KEYWORDS

surfactants, polymers, nanostars, surface adsorption, plasmonic nanoparticles, gold

1 Introduction

Surfactants and polymers are frequently utilized as shape-directing agents in the synthesis of colloidal anisotropic noble metal nanoparticles (Song et al., 2021; González-Rubio et al., 2020). Their critical role in achieving anisotropy is well known (Tao et al., 2008; Sau and Rogach, 2010; Xiao and Qi, 2011), and many studies (Bakshi, 2016; Bhattacharya and Biswas, 2011; Guan et al., 2023; Phan and Nguyen, 2017) have been conducted to understand the nature and the dynamics of their interactions with the surface of the growing crystal. For historical reasons that are amplified by the simplicity of the shape, nanorods occupy a prominent spot in such literature (Burrows et al., 2016; Greskovich et al., 2023; Lohse and Murphy, 2013; Nikoobakht and El-Sayed, 2003; Zheng et al., 2021). However, nanoparticles of more complex shapes, such as nanostars, currently stand out as the benchmark morphology for high-sensitivity and high-performance applications (Ngo et al., 2022), raising interest for nanostars-specific surfactant dynamics. While attention has been directed to the mechanistic aspects related to the role of surfactants in the generation of these branched nanoparticles (Zhou et al., 2015; Wang et al., 2019; Abu Serea et al., 2024), the multitude of applications in which they are used (Abu Serea et al., 2024) imposes the need to characterize the final, *mature* surface landscape of the nanostructure, as it has been done for nanorods in recent years (Mosquera et al., 2023). Therefore, it is important to discern which characterization approaches can be reasonably translated from the existing nanorod literature, and what must be uniquely addressed for the star-shaped morphology instead.

Many ligand-mediated syntheses of nanostars have been developed (in this work, we will refer to the ensemble of surfactants and polymers with the term ligands) and different ligands have been exploited, such as Cetyltrimethylammonium Bromide (CTAB), Polyvinylpyrrolidone (PVP),

10.3389/fnano.2024.1505304

TABLE 1 Properties of the most common ligands employed in the synthesis of plasmonic nanostars.

Ligand	Category	Molecular structure	Solubility [g·l^{-1}]	CMC$_1$ [mM]	N$_{agg1}$	CMC$_2$ [mM]	N$_{agg2}$
SDS	anionic surfactant	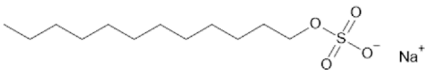	Toluene: 0.3, Methyl tert-Butyl Ether: >588, ethyl acetate: >588, methyl ethyl ketone: >588, isobutyl alcohol: >588, water: >588 (Pollard et al., 2006)	8.0–9.0 (Emerson and Holtzer, 1967; Chang and Kaler, 1985; Bahri et al., 2006)	n.d	65–70 (Kodama et al., 1972; Shi et al., 2011)	83–96 (Prévost and Gradzielski, 2009)
CTAB	cationic surfactant	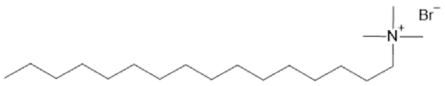	Methyl ethyl ketone: 1.3, isobutyl alcohol: 30.7, water: 3.1 (Pollard et al., 2006)	0.8–1.1 (Bahri et al., 2006; Tedeschi et al., 2003; Li et al., 1997)	n.d	20 (Shi et al., 2011)	144 (Berr, 1987)
Triton X-100	nonionic surfactant	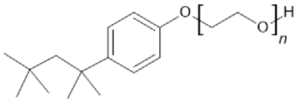	Toluene: >649, methyl tert-butyl ether: >649, ethyl acetate: >649, methyl ethyl ketone: >649, isobutyl alcohol: >588, water: >865 (Pollard et al., 2006)	0.22–0.25 (Tiller et al., 1984; Møller and le Maire, 1993)	~30 (De Nicola et al., 2015)	n.d	n.d
PVP	polymer	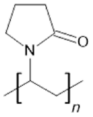 molecular weight range ranges from 2,500 to approximately 1 million g·mol^{-1} (Haaf et al., 1985)	Water, methanol, ethanol, propanol, butanol, cyclohexanol, chloroform, dichloromethane, 1,2-dichloroethane, N-methylpyrrolidone, ethylenediamine, Di(ethylene glycol), Poly (ethylene glycol) 400, propylene glycol, 1,4-butanediol, Glycerol, N-vinylpyrrolidone, triethanolamine, formic acid, acetic acid, propionic acid (Haaf et al., 1985)	-	-	-	-

Sodium Dodecyl Sulfate (SDS), and Triton X-100 (Senthil Kumar et al., 2008; Atta et al., 2019; Bazán-Díaz et al., 2015; Chatterjee et al., 2018). As previously mentioned, it is generally accepted that ligands preferentially passivate certain crystalline facets of the growing crystal, leading to symmetry breaking, and thus, to the growth of anisotropic morphologies (González-Rubio et al., 2020; Pedrazo-Tardajos et al., 2024). While it is possible to synthesize nanostars without the aid of ligands (Yuan et al., 2012; Lu et al., 2016; Chandra et al., 2016; Deriu et al., 2022), their presence helps to slow down the reaction (He et al., 2014), thus reasonably improving morphology control and final product homogeneity. Because a high level of morphological homogeneity is crucial to the development of some emerging applications, such as plasmon-driven catalysis (Cui et al., 2015; Atta et al., 2018; Ma and Liang, 2020) or microvolume and single nanoparticle experiments in Surface Enhanced Raman Spectroscopy (SERS) (Dondapati et al., 2010; Rodríguez-Lorenzo et al., 2019; Ke et al., 2024), there are instances in which the presence of a ligand in the colloidal formulation cannot be avoided. In both SERS sensing and plasmon-sustained catalysis, the nanoparticle surface landscape represents the physical domain where the processes take place; therefore, it becomes fundamental to characterize ligand-surface interactions, both spatially and energetically, such that surface clean-up protocols can be rationally implemented (Song et al., 2021; Pu et al., 2022),

In this mini-review we present traditional and cutting-edge characterization methods useful for energetic, spatial, and conformational elucidation of ligand-surface interactions occurring on mature nanostars. Due to the emerging nature of such analytical interest, we approach the discussion by utilizing the nanorod literature as a starting point, highlighting applicability and challenges intrinsic in the translation of those methods to nanostar systems.

2 Overview of common surfactants and polymers utilized in plasmonic nanostar colloids

Surfactants are *amphipathic* molecules characterized by a structural group with low affinity to the solvent (*lyophobic*) and a

group with high affinity to it *(lyophilic)* (Rosen, 1989; Cullum, 1994; Goyal and Aswal, 2001). Above the first critical micellar concentration (CMC_1) (Perinelli et al., 2020), surfactants start to organize themselves into supramolecular structures called *micelles*, exposing the lyophilic groups towards the solvent. In surfactant-mediated syntheses, the concentration of the surfactant is usually above its CMC_1, therefore, both growing crystals and mature nanoparticles reasonably interact with the surfactant as a supramolecular aggregate rather than with its free molecular form. The shape of micelles can evolve with increasing surfactant concentration, and the surfactant concentration also influences the aggregation number of the supramolecular entity, that is, the number of molecules per micelle (N_{agg}). A second critical micellar concentration (CMC_2) can be defined, corresponding to the concentration at which the growth of the micelle is more sensitive to concentration increments, thus leading to rapid shape transitions from spherical to elliptical or rod-like morphologies (Magnus, 2016).

Unlike surfactants, polymers typically do not form micelles, and their shape-directing action is usually modulated by their molecular weight. Recent studies on the energetics of metal-PVP interactions (Ye et al., 2021) have demonstrated a direct dependence between PVP molecular weight and particle-averaged absorption equilibrium constant, validating the use of different molecular weights in nanoparticle shape control. Nevertheless, polymers might still experience conformational changes due to concentration and solvent effects. For example, the change in non-covalent interactions within PVP sub-domains with varying solvent system was reported to produce observable conformational changes that alter the polymer packing density on the surface (Yang et al., 2021). The main properties of the most common ligands utilized in colloidal nanostar synthesis, SDS, CTAB, Triton X-100 and PVP, are summarized in Table 1.

SDS, CTAB, and Triton X-100 micellar shape and hydration are strongly influenced by the presence of salts in the solution. This property must be taken into consideration because, in a colloidal system, nanoparticles coexist with solutes resulting from the synthetic process; the concentration of solutes in a colloid may vary with different preparations and clean-up procedures, thus influencing the micellar architecture that is interacting with the surface of the nanoparticles. Micellar shape alteration with salt content can be observed by small-angle X-ray scattering (SAXS) and small-angle neutron scattering (SANS); the first exploits the contrast in the scattering signal of X-rays to discriminate between spatial fluctuations in the electron density of different atoms, while the second utilizes the contrast in the scattering signal of neutrons to discriminate between different atomic nuclei (Narayanan, 2009). As an example, time-resolved SAXS study of SDS in the presence of various concentrations of sodium chloride evidenced that the salt causes an electrostatic screening of the SDS head groups, leading to the formation of more elongated supramolecular worm-like micellar structures (Jensen et al., 2014). Interestingly, the supramolecular arrangement of SDS is also susceptible to the *type* of salt added to the solution, as demonstrated through SANS measurements (Prévost and Gradzielski, 2009). Similar effects were also observed for CTAB by volumetric and fluorescence studies (Yue et al., 2000). It is reasonable to say that the hydration level of the cationic component of the salt plays an important role in modulating such salt-type-dependent shape alterations of micelles, as demonstrated for Triton X-100 by light scattering measurements and density studies (Molina-Bolívar et al., 2002). The micelle hydration decreases both in the presence of more hydrated cations and with increasing salt concentration, causing a collapse of the micellar hydrophilic chains, as well as an increase in N_{agg}, with consequent mechanical entrapment of more water molecules (Molina-Bolívar et al., 2002).

3 Ligand-metal interactions

A quantitative evaluation of ligand-metal interactions is essential for enhancing the control of processes occurring on nanostructured surfaces (Ye et al., 2021; Bae et al., 2021). A complete characterization for this scope would include the evaluation of the energetics together with the spatial configuration adopted by the ligand on a specific location on the surface of the nanoparticle as well as the ligand coverage density on the total nanoparticle exposed surface. Such a level of in-depth surface characterization is technologically challenging, even for the more regular shapes like spheres, rods, and plates (Wu et al., 2019), and the simultaneous presence of flat, concave, and convex surfaces that characterizes star-shaped nanoparticles intensifies the challenge (Bae et al., 2021; Xi et al., 2024). Indeed, identical crystalline facets differing only in surface curvature can exhibit different adsorption affinity for the same ligand, leading to a pronounced adsorbate patchiness on the surface (Ye et al., 2021; Bae et al., 2021; Villarreal et al., 2017; Walker et al., 2013).

In the following sections, we review the most common techniques for studying ligand-metal interactions, including advances in imaging techniques, and other innovative surface characterization approaches. It is important to anticipate that the reader will encounter many examples pertaining to nanorod literature. The reason of such a preponderance is both historical and technical—the earlier establishment of finely controlled nanorods and the higher simplicity of their shape ultimately result in an overwhelming majority of surface chemistry studies focusing on nanorods rather than nanostars. Because there is a "morphological affinity" between rod-like and star-like nanostructures (*i.e.*, nanostars can be seen as a collection of rods, and tips in general can be considered rod-like structures), we believe that surface characterization methods as applied to nanorods can be utilized as a starting point to investigate nanostar systems. It should be pointed out that the complexity of the star shape can pose specific analytical challenges and cannot always be neglected; therefore, nanostar-specific method transferability and challenges will be systematically discussed.

3.1 Bulk techniques

The techniques typically used to quantify adsorbed ligands on plasmonic nanostructures are bulk techniques, and as such they provide average, non-spatially resolved quantities as the output. As an example, such quantities could be the ligand shell thickness or the energetics parameters that characterize ligand-metal binding. While methods such as surface plasmon resonance (SPR) and isothermal

titration calorimetry (ITC) are popular for the above-mentioned characterizations, they are most suitable to non-native ligands, because they require that the ligand of interest is not already present on the nanoparticle surface (Vilain et al., 2007; Prozeller et al., 2019; Ong et al., 2017; Greytak et al., 2022; Mishra and Das, 2022). On the other hand, the already mentioned SANS and SAXS can be exploited to estimate the average native surfactant shell thickness, as done, for example, for CTAB-capped gold nanorods (Gómez-Graña et al., 2012). Another well-established bulk analytical technique is thermogravimetric analysis (TGA), which allows to quantify the percentage of organic compounds presents in hybrid organic-inorganic systems by monitoring the mass change in the sample with temperature (Agasti et al., 2008; Saadatkhah et al., 2020). As a proof of the historical establishment of TGA, we cite the work by Vigderman et al. (2012), in which TGA was used to quantify the ligand surface density of CTAB-synthesized colloidal nanorods after ligand exchange with (16-mercaptohexadecyl)trimethylammonium bromide (MTAB). By combining the electron microscopy-derived average surface area per nanorod with the TGA results, the average coverage density of MTAB per nanorod was estimated. Compared to nanorods, nanostars are more prominently developed in the three-dimensional space, rendering the reconstruction of the relative position of their volumetric subunits (*i.e.*, branches and core) from TEM 2D projections particularly challenging. However, the translation of the nanorod TGA-TEM method to nanostars would only require the absolute estimate of the nanoparticle surface; as demonstrated by Tsoulos et al. (2017), this parameter can be calculated from TEM images, by extracting the core radius, the average radius of curvature of the nanostar tips, the base radius of the spikes, and the distance between the latter two radii.

Another bulk technique typically used to gain information about the structure, dynamics, and chemical environment of ligands interacting with nanoparticles is proton nuclear magnetic resonance (^{1}H NMR) (Marbella and Millstone, 2015). This technique enables the measurement of the spin property of a nucleus, correlating it to the intra- and inter-molecular environment (Fan and Lane, 2016). For this reason, it is possible to determine the ligand identity, quantity, and patchiness (Marbella and Millstone, 2015). Interestingly, it is in principle possible to obtain insights also on the spatial distribution of adsorbed ligands along different directions in an anisotropic nanoparticle because the amplitudes of the characteristic chemical shifts of a ligand change in relation to the ligand packing density. If the latter is significantly different for surface regions with different curvature, it is expected to be detectable on the ^{1}H NMR spectrum as non-overlapping peaks, due to the different local chemical environments. This rationale was utilized by Wu et al. (2019) to quantitatively evaluate the packing and coverage density of a thiolated ligand on colloidal gold nanorods with different aspect ratios. A lower aspect ratio nanorod has shorter sides, and therefore, higher edge influence in the ^{1}H NMR signal; as previously said, this characteristic modifies the amplitude of the chemical shifts of an investigated ligand if it exhibits an anisotropic packing density. It needs to be pointed out that, for such a distinction to be observable, the nanoparticles on which the ligands are adsorbed must be sufficiently small to avoid the typical NMR band broadening effects that depend on nanoparticle size. Therefore, the application of *in situ* ^{1}H NMR to the study of ligands on nanostars could be hindered by the dimension of the nanostars themselves, which are typically around 70–200 nm from tip to tip (Atta et al., 2019; Pallavicini et al., 2013; He et al., 2015).

3.2 Electron microscopy advancements

In recent years, the characterization of ligand-metal interactions advanced significantly, moving toward spatially resolved measurements at the nanoscale. Janicek et al. (2019) employed electron energy loss spectroscopy (EELS) within an aberration-corrected scanning transmission electron microscope (STEM) to directly visualize and quantify CTAB distribution on gold nanorods. Such a pioneering study was enabled by the use of graphene TEM grids for sample deposition. Graphene was already known to enhance the signal to noise ratio of organic components at hard interfaces (Lee et al., 2009) and to preserve structurally sensitive materials and features from electron beam damage (Algara-Siller et al., 2013). This sample preparation in conjunction with STEM-EELS mapping allowed for the estimate of the binding density of CTAB, revealing a decrease near the nanorod edges. The same method was utilized by Bae et al. (2021) to investigate the adsorption of unmethylated cytosine-phosphate-guanine (CpG) DNA strands on gold nanostars, providing evidence that STEM-EELS mapping with sample deposition on graphene TEM grids is applicable to nanostar systems. In the study by Bae et al. (2021), it was found that the CpG binding density was higher on convex surfaces (*i.e.*, the tips) compared to flat surfaces, while the study was inconclusive as to the binding density at concave surfaces (*i.e.*, tip-core junctions).

In all microscopy-involving studies cited so far, as well as in the most common TEM microscope setups, the sample is in a dried or cryogenic state. The capillary forces generated during drying or cryogenic treatment are likely to cause collapse and distortion of the native ligand configuration on the surface (Pedrazo-Tardajos et al., 2024). Colloidal nanoparticles exist in a solution environment, and thus, the visualization of ligand shells in dried samples leads to an intrinsic limitation in the ability to accurately preserve the native and dynamic conformation of the colloidal nanoparticle-ligand pair. To address the challenge of imaging colloidal nanoparticles in their native liquid matrix, graphene liquid cell electron microscopy (GLC-EM) has recently emerged (Yuk et al., 2012). GLC-EM is a cutting-edge liquid-phase EM technique that received strong attention in the last 5 years, due to its ability to visualize the dynamics of the interactions between ligands and metallic nanostructures. Pedrazo-Tardajos et al. (2024) recently published a very innovative work using GLC-EM to visualize the composition, anisotropy, and dynamics of the CTAB distribution on gold nanorod surfaces. Images and videos of the CTAB shell adsorbed on a single nanorod were recorded, and the influence of the amount of liquid present in the cell on the adsorbate relaxation and contraction was investigated. For GLC-EM measurements with a GLC thickness in the highest end of the investigated range (*i.e.*, 30–95 nm), the authors found that the CTAB shell width was expanded compared to the determinations performed in GLCs with lower liquid volumes, thus reasonably better mimicking the CTAB configuration in the native environment. Moreover, the ability to generate videos allowed for the visualization of the

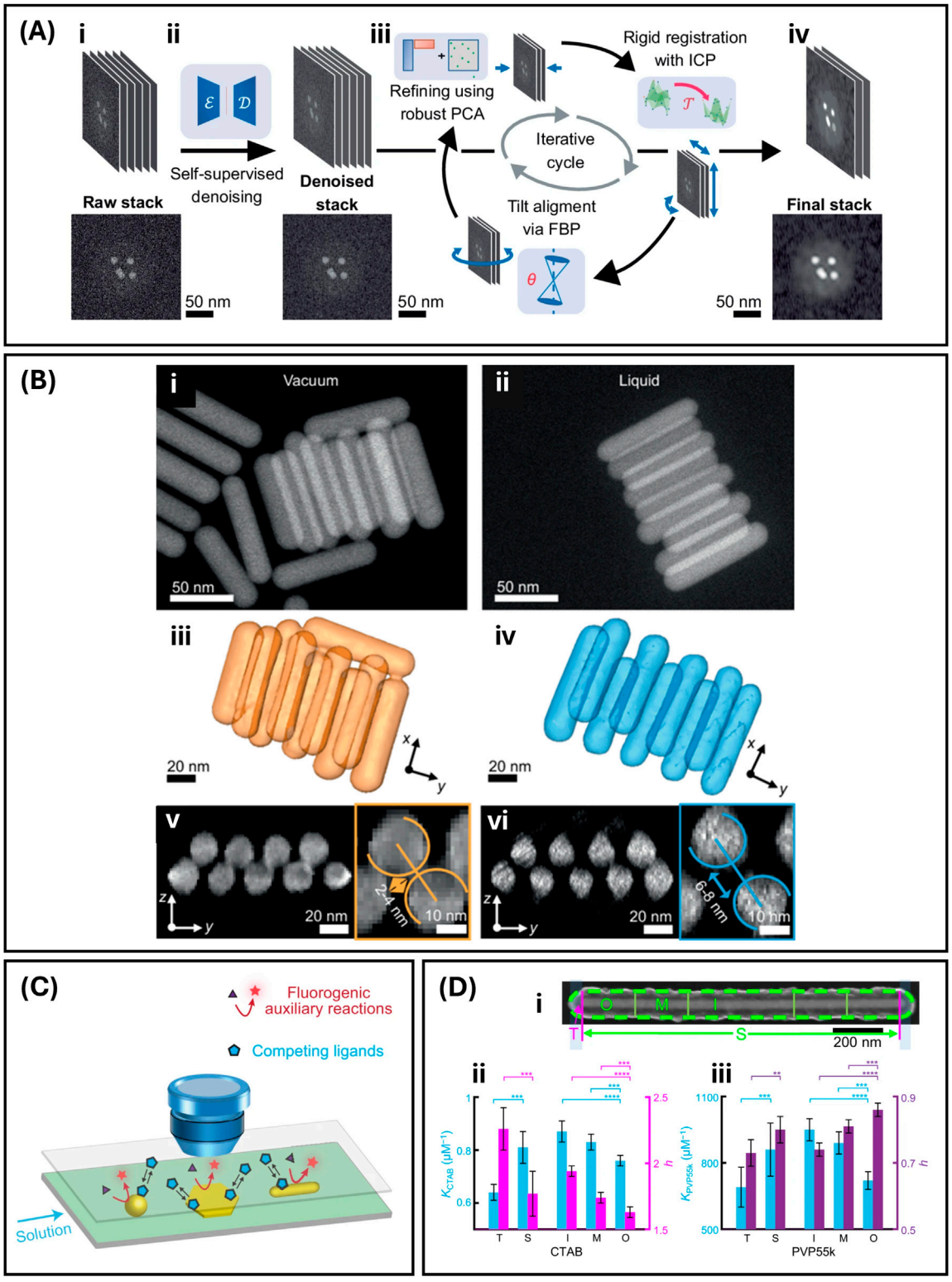

FIGURE 1
Overview of novel approaches for the visualization and the characterization of ligand-metal interactions in colloidal nanoparticles. **(A)** Pre-processing workflow of a fast electron tomography tilt series. (i) Illustration of raw tilt series and an example of raw image. (ii) Representation of the self-supervised denoising method using convolutional autoencoders (CAE). Ɛ symbolizes the encoder convolutional neural network (CNN) architecture while Ɗ is the decoder CNN. In addition to this, an example of denoised image is shown. (iii) Scheme of the implemented iterative process: improvement of the tilt series employing robust principal component analysis (RPCA), rigid registration through the iterative closest point (ICP) method (Ƭ symbolizes the rigid transformation operator), and tilt-axis alignment using filtered back projection (FBP). The value of the angular shift needed to correct the tilt alignment is indicated by θ. (iv) The final refined, aligned, and denoised stack, with a real image as example. **(B)** Comparison of bilayer assemblies of Au nanorods (NRs) in vacuum and liquid environments. 2D HAADF-STEM images of self-organized Au NRs observed (i) in vacuum and (ii) in liquid. (iii, iv) 3D
(*Continued*)

FIGURE 1 (Continued)
reconstructions and (v,vi) orthogonal projections of NR superlattices in vacuum (iii, v) and liquid (iv, vi). Insets show close-up views of two adjacent Au NRs, highlighting the difference in surface-to-surface spacing between the (v) vacuum and (vi) liquid conditions. Reproduced from Arenas Esteban et al. (2024). **(C)** Schematic representation of COMPEITS experimental design. Adapted from Ye et al. (2021). **(D)** COMPEITS results on nanorods. (i) SEM image of a nanorod and its two schemes of segmentation: side facet (S) and tips (T), outer (O), middle (M), and inner (I) regions from the tip toward the center. Average values of K and h for (ii) CTAB and (iii) 55k PVP for the identified regions. h is the Hill coefficient of cooperativity: h > 1 indicates positive cooperativity while h < 1 negative cooperativity. **p < 0.01; ***p < 0.001; ****p < 0.05); paired Student's t-test. Error bars are the standard error of the mean. Adapted from (Ye et al., 2021).

dynamic nature of adsorbates in colloids, which are by nature not static.

TEM imaging of branched morphologies suffers from the two-dimensionality imposed by the technique. To observe the true volumetric nature of nanostars, it might be necessary to perform *tomographic* measurements instead, which are unfortunately known to be extremely time consuming, and thus, resource intensive. A pioneering approach that overcomes this limitation while simultaneously addressing the need to operate in the native colloidal environment, was demonstrated by Arenas Esteban et al. (2024), who implemented liquid fast electron tomography (LP fast ET). The uniqueness of this study is the implementation of a method that integrates fast data acquisition in a commercial liquid cell with a customized alignment and reconstruction workflow (Figure 1A) that sensibly decreases acquisition times. This approach was tested on an assembly of CTAB-capped gold nanorods as the model system and allowed for the determination of the native interparticle distance in the system (Figure 1B). The acquisition time of an LP fast ET experiment is about 1/15 of the time required by traditional acquisition methods, showing great potential for the nanostar-morphology parametrization both in the three-dimensional space *and* in the colloidal native state.

3.3 State-of-the-art quantitative experimental techniques with nanoscale resolution and computational simulations

Advanced TEM setups and associated spectroscopies allow to visualize the morphology of ligands adsorbed on the surface of colloidal metal nanoparticles and provide information on the spatial distribution of elements (*i.e.*, EELS). However, they are unable to quantify the related energetics. For colloidal nanoparticles, the measurement of these quantities is as fundamental as it is extremely difficult. A novel approach to this challenge is presented by Ye et al. (2021) with the employment of competition-enabled imaging technique with super-resolution (COMPEITS). This technique, schematized in Figure 1C, allows for the *in situ* imaging of first-layer non-fluorescent surface processes with nanometer resolution, by exploiting the competition with a surface-catalyzed fluorogenic auxiliary reaction (Mao et al., 2019). Using single-molecule fluorescence microscopy, the products of the auxiliary reaction are detected, and their associated information is used to build a map of surface reactivity and extract thermodynamic parameters, such as the adsorption constant and cooperativity. The authors utilized the devised methodology to investigate adsorption energetics on gold nanorods of CTAB and 55k PVP (*i.e.*, molecular weight ~55k g·mol^{-1}), and a correlation between the surface defect density and the particle-averaged absorption equilibrium constant (K) was found. Both for CTAB and 55k PVP, the K increases toward the nanorod center because of the increase in surface defect density (Figure 1D).

It must be noted that the ligand concentrations used for the COMPEITS titrations are lower than what normally present on the *as synthesized* nanoparticles. For example, the concentration of CTAB is below the CMC_1, therefore, an evaluation of the capability of COMPEITS to handle surfactant interaction determinations while in the micellar state is presently not available. When assessing the transferability of the technique to nanostar systems, it must also be added that the effective resolution range of COMPEITS is reported to be between 10 and 40 nm, thus potentially limiting applicability from a visualization standpoint, as nanostar tips typically present finer dimensions.

Computational modeling and simulations are very powerful tools for studying the interaction dynamics of soft-hard matter, both to elucidate mechanistic aspects relative to such phenomena, and to reach nanoscale insight where the current technological capabilities do not allow for experimental determinations. Because colloidal nanoparticle systems are inherently very large and complex, and because their truthful representation should ideally include the presence of a solvent, it is typically too computationally expensive to approach the problem at a pure atomistic level. Multiscale modeling methods provide a computationally affordable way to access complex, often solvated systems, by combining finer-scale computational models (*e.g.*, atomistic) with less computationally expensive ones (*e.g.*, molecular dynamics, coarse-grain models) (Peter and Kremer, 2009; Fish et al., 2021). For example, multiscale modeling has been used to study the supramolecular organization of aqueous solutions of surfactants such as Triton X-100 (De Nicola et al., 2015). A library of atomistic models of Triton X-100 individual molecules in different rotational configurations was obtained and utilized to refine a coarse-grained model of the micellar structure by reverse mapping procedure, thus minimizing the computational cost (De Nicola et al., 2015), Gao et al. (2018) developed a multiscale simulation model to explore the molecular structure and packing density of CTAB, as well as its adsorption kinetics when adsorbed on three different gold facets, shaped as infinite planar surfaces. More recently, De Angelis et al. (2019) applied a multiscale modelling approach to the study of SDS adsorption on alumina nanospheres, revealing the influence of nanoscale surface curvature in driving surfactant adsorption dynamics. The application of this approach to simulate surfactant adsorption dynamics on star-shaped morphologies could be a powerful tool to detect the presence of different adsorption sites, since both convex and concave surfaces need to be modeled (Wen et al., 2021).

4 Discussion

Because the plasmonic properties of nanostars are intrinsically sustained at the surface level, knowledge of the modes and energies of the interactions that are established on the surface by capping ligands is of broad interest, spanning not only the fundamental science community, but also many application-oriented fields. For example, sensing based on direct SERS relies on the adsorption of analytes to the plasmon-sustaining surface, rendering an in-depth characterization of the energies and spatial patchiness of pre-adsorbed species (*e.g.*, ligands) indispensable to the high-end optimization of the analytical performances (Deriu et al., 2022). Analogous characterizations are also useful in plasmon-driven catalysis, where electron transfer might be impeded or modulated by the presence of interfacial ligands (Lu et al., 2021; Smith and Jain, 2016), thus making knowledge of their surface interactions a critical element to push the boundaries of both reaction yields and catalyst lifetime.

In the previous sections, we have utilized the more established nanorod literature to highlight which characterization methods are available for the elucidation of such metal-molecule interactions and how they can be translated to nanostars systems, discussing the challenges and limitations inherent to this shape. It is worth reminding the reader that, while the development of characterization techniques with nanoscale resolution is necessary to the advancement of fundamental knowledge of phenomena at the nanoscale, from a strictly practical viewpoint, it is also true that, in certain circumstances, bulk techniques might provide all of the necessary information to unlock the full potential of a given nanostar-based application. Lastly, where the technological implementations do not allow for the direct measurement of properties, or when the experimental implementations are prohibitive, computational models and simulations can provide a valid resource to investigate the systems anyways, or to explore and validate mechanistic interpretations of experimental results.

With this mini-review, we invite the reader to appreciate the great potential that lies in the integrated use of characterization techniques for the elucidation and visualization of metal-ligand interactions, and we hope to spark ideas on how to exploit such potential to further advance both nanostars technological applications, and the characterization approaches themselves.

Author contributions

DF: Writing–original draft. CD: Writing–original draft. LF: Writing–review and editing.

Funding

The author(s) declare that financial support was received for the research, authorship, and/or publication of this article. This project has received funding from the European Research Council (ERC) under the European Union's Horizon 2020 research and innovation programme (grant agreement No 865819).

Conflict of interest

The authors declare that the research was conducted in the absence of any commercial or financial relationships that could be construed as a potential conflict of interest.

Generative AI statement

The author(s) declare that no Generative AI was used in the creation of this manuscript.

Publisher's note

References

Abu Serea, E. S., Berganza, L. B., Lanceros-Méndez, S., and Reguera, J. (2024). Cu 2+ –assisted synthesis of ultrasharp and sub-10 nm gold nanostars. Applications in catalysis, sensing, and photothermia. *ACS Appl. Nano Mat.* 7 (16), 19416–19426. doi:10.1021/acsanm.4c03310

Agasti, S. S., You, C.-C., Arumugam, P., and Rotello, V. M. (2008). Structural control of the monolayer stability of water-soluble gold nanoparticles. *J. Mater Chem.* 18 (1), 70–73. doi:10.1039/b711434f

Algara-Siller, G., Kurasch, S., Sedighi, M., Lehtinen, O., and Kaiser, U. (2013). The pristine atomic structure of MoS2 monolayer protected from electron radiation damage by graphene. *Appl. Phys. Lett.* 103 (20). doi:10.1063/1.4830036

Arenas Esteban, D., Wang, D., Kadu, A., Olluyn, N., Sánchez-Iglesias, A., Gomez-Perez, A., et al. (2024). Quantitative 3D structural analysis of small colloidal assemblies under native conditions by liquid-cell fast electron tomography. *Nat. Commun.* 15 (1), 6399. doi:10.1038/s41467-024-50652-y

Atta, S., Beetz, M., and Fabris, L. (2019). Understanding the role of AgNO 3 concentration and seed morphology in the achievement of tunable shape control in gold nanostars. *Nanoscale* 11 (6), 2946–2958. doi:10.1039/c8nr07615d

Atta, S., Pennington, A. M., Celik, F. E., and Fabris, L. (2018). TiO2 on gold nanostars enhances photocatalytic water reduction in the near-infrared regime. *Chem.* 4 (9), 2140–2153. doi:10.1016/j.chempr.2018.06.004

Bae, S. hyun, Huang, P., Lee, K., and Odom, T. (2021). Curvature-dependent organic ligand binding on gold nanostars revealed by quantitative EELS spectral imaging. *Microsc. Microanal.* 27 (S1), 3320–3322. doi:10.1017/s1431927621011429

Bahri, M. A., Hoebeke, M., Grammenos, A., Delanaye, L., Vandewalle, N., and Seret, A. (2006). Investigation of SDS, DTAB and CTAB micelle microviscosities by electron spin resonance. *Colloids Surfaces A Physicochem Eng. Asp.* 290 (1–3), 206–212. doi:10.1016/j.colsurfa.2006.05.021

Bakshi, M. S. (2016). How surfactants control crystal growth of nanomaterials. *Cryst. Growth Des.* 16 (2), 1104–1133. doi:10.1021/acs.cgd.5b01465

Bazán-Díaz, L., Mendoza-Cruz, R., Velázquez-Salazar, J. J., Plascencia-Villa, G., Romeu, D., Reyes-Gasga, J., et al. (2015). Gold–copper nanostars as photo-thermal agents: synthesis and advanced electron microscopy characterization. *Nanoscale* 7 (48), 20734–20742. doi:10.1039/c5nr06491k

Berr, S. S. (1987). Solvent isotope effects on alkytrimethylammonium bromide micelles as a function of alkyl chain length. *J. Phys. Chem.* 91 (18), 4760–4765. doi:10.1021/j100302a024

Bhattacharya, S., and Biswas, J. (2011). Role of spacer lengths of gemini surfactants in the synthesis of silver nanorods in micellar media. *Nanoscale* 3 (7), 2924. doi:10.1039/c1nr10141b

Burrows, N. D., Lin, W., Hinman, J. G., Dennison, J. M., Vartanian, A. M., Abadeer, N. S., et al. (2016). Surface chemistry of gold nanorods. *Langmuir* 32 (39), 9905–9921. doi:10.1021/acs.langmuir.6b02706

Chandra, K., Culver, K. S. B., Werner, S. E., Lee, R. C., and Odom, T. W. (2016). Manipulating the anisotropic structure of gold nanostars using good's buffers. *Chem. Mater* 28 (18), 6763–6769. doi:10.1021/acs.chemmater.6b03242

Chang, N. J., and Kaler, E. W. (1985). The structure of sodium dodecyl sulfate micelles in solutions of water and deuterium oxide. *J. Phys. Chem.* 89 (14), 2996–3000. doi:10.1021/j100260a009

Chatterjee, H., Rahman, D. S., Sengupta, M., and Ghosh, S. K. (2018). Gold nanostars in plasmonic photothermal therapy: the role of tip heads in the thermoplasmonic landscape. *J. Phys. Chem. C* 122 (24), 13082–13094. doi:10.1021/acs.jpcc.8b00388

Cui, Q., Xia, B., Mitzscherling, S., Masic, A., Li, L., Bargheer, M., et al. (2015). Preparation of gold nanostars and their study in selective catalytic reactions. *Colloids Surfaces A Physicochem Eng. Asp.* 465, 20–25. doi:10.1016/j.colsurfa.2014.10.028

Cullum, D. C. (1994). Surfactant types; classification, identification, separation. *Introd. Surfactant Analysis*, 17–41. doi:10.1007/978-94-011-1316-8_2

De Angelis, P., Cardellini, A., and Asinari, P. (2019). Exploring the free energy landscape to predict the surfactant adsorption isotherm at the nanoparticle–water interface. *ACS Cent. Sci.* 5 (11), 1804–1812. doi:10.1021/acscentsci.9b00773

De Nicola, A., Kawakatsu, T., Rosano, C., Celino, M., Rocco, M., and Milano, G. (2015). Self-assembly of Triton X-100 in water solutions: a multiscale simulation study linking mesoscale to atomistic models. *J. Chem. Theory Comput.* 11 (10), 4959–4971. doi:10.1021/acs.jctc.5b00485

Deriu, C., Bracho, A., and McCord, B. (2022). Tailored colloidal nanostars for surface-enhanced Raman spectroscopy: optimization of formulation components and study of the stabilizer–nanoparticle interactions. *J. Phys. Chem. C* 126 (4), 2023–2040. doi:10.1021/acs.jpcc.1c08145

Dondapati, S. K., Sau, T. K., Hrelescu, C., Klar, T. A., Stefani, F. D., and Feldmann, J. (2010). Label-free biosensing based on single gold nanostars as plasmonic transducers. *ACS Nano* 4 (11), 6318–6322. doi:10.1021/nn100760f

Emerson, M. F., and Holtzer, A. (1967). On the ionic strength dependence of micelle number. II. *J. Phys. Chem.* 71 (6), 1898–1907. doi:10.1021/j100865a057

Fan, T. W. M., and Lane, A. N. (2016). Applications of NMR spectroscopy to systems biochemistry. *Prog. Nucl. Magn. Reson Spectrosc.* 92–93, 18–53. doi:10.1016/j.pnmrs.2016.01.005

Fish, J., Wagner, G. J., and Keten, S. (2021). Mesoscopic and multiscale modelling in materials. *Nat. Mat.* 20 (6), 774–786. doi:10.1038/s41563-020-00913-0

Gao, H.-M., Liu, H., Qian, H.-J., Jiao, G.-S., and Lu, Z.-Y. (2018). Multiscale simulations of ligand adsorption and exchange on gold nanoparticles. *Phys. Chem. Chem. Phys.* 20 (3), 1381–1394. doi:10.1039/c7cp07039j

Gómez-Graña, S., Hubert, F., Testard, F., Guerrero-Martínez, A., Grillo, I., Liz-Marzán, L. M., et al. (2012). Surfactant (Bi)layers on gold nanorods. *Langmuir* 28 (2), 1453–1459. doi:10.1021/la203451p

González-Rubio, G., Scarabelli, L., Guerrero-Martínez, A., and Liz-Marzán, L. M. (2020). Surfactant-Assisted symmetry breaking in colloidal gold nanocrystal growth. *ChemNanoMat* 6 (5), 698–707. doi:10.1002/cnma.201900754

Goyal, P. S., and Aswal, V. K. (2001). Micellar structure and inter-micelle interactions in micellar solutions: results of small angle neutron scattering studies. *Curr. Sci.* 80 (8), 972–979.

Greskovich, K. M., Powderly, K. M., Kincanon, M. M., Forney, N. B., Jalomo, C. A., Wo, A., et al. (2023). The landscape of gold nanocrystal surface chemistry. *Acc. Chem. Res.* 56 (12), 1553–1564. doi:10.1021/acs.accounts.3c00109

Greytak, A. B., Abiodun, S. L., Burrell, J. M., Cook, E. N., Jayaweera, N. P., Islam, M. M., et al. (2022). Thermodynamics of nanocrystal-ligand binding through isothermal titration calorimetry. *Chem. Commun.* 58 (94), 13037–13058. doi:10.1039/d2cc05012a

Guan, H., Harris, C., and Sun, S. (2023). Metal–ligand interactions and their roles in controlling nanoparticle formation and functions. *Acc. Chem. Res.* 56 (12), 1591–1601. doi:10.1021/acs.accounts.3c00156

Haaf, F., Sanner, A., and Straub, F. (1985). Polymers of N-vinylpyrrolidone: synthesis, characterization and uses. *Polym. J.* 17 (1), 143–152. doi:10.1295/polymj.17.143

He, R., Wang, Y.-C., Wang, X., Wang, Z., Liu, G., Zhou, W., et al. (2014). Facile synthesis of pentacle gold–copper alloy nanocrystals and their plasmonic and catalytic properties. *Nat. Commun.* 5 (1), 4327. doi:10.1038/ncomms5327

He, S., Kang, M. W. C., Khan, F. J., Tan, E. K. M., Reyes, M. A., and Kah, J. C. Y. (2015). Optimizing gold nanostars as a colloid-based surface-enhanced Raman scattering (SERS) substrate. *J. Opt.* 17 (11), 114013. doi:10.1088/2040-8978/17/11/114013

Janicek, B. E., Hinman, J. G., Hinman, J. J., Bae, S. H., Wu, M., Turner, J., et al. (2019). Quantitative imaging of organic ligand density on anisotropic inorganic nanocrystals. *Nano Lett.* 19 (9), 6308–6314. doi:10.1021/acs.nanolett.9b02434

Jensen, G. V., Lund, R., Gummel, J., Narayanan, T., and Pedersen, J. S. (2014). Monitoring the transition from spherical to polymer-like surfactant micelles using small-angle X-ray scattering. *Angew. Chem. Int. Ed.* 53 (43), 11524–11528. doi:10.1002/anie.201406489

Ke, Q., Yin, L., Jayan, H., El-Seedi, H. R., Zou, X., and Guo, Z. (2024). Ag-coated tetrapod gold nanostars (Au@AgNSs) for acetamiprid determination in tea using SERS combined with microfluidics. *Anal. Methods* 16 (17), 2721–2731. doi:10.1039/d4ay00297k

Kodama, M., Kubota, Y., and Miura, M. (1972). The second CMC of the aqueous solution of sodium dodecyl sulfate. III. Light-Scattering. *Bull. Chem. Soc. Jpn.* 45 (9), 2953–2955. doi:10.1246/bcsj.45.2953

Lee, Z., Jeon, K.-J., Dato, A., Erni, R., Richardson, T. J., Frenklach, M., et al. (2009). Direct imaging of Soft–Hard interfaces enabled by graphene. *Nano Lett.* 9 (9), 3365–3369. doi:10.1021/nl901664k

Li, F., Li, G.-Z., Wang, H.-Q., and Xue, Q.-J. (1997). Studies on cetyltrimethylammonium bromide (CTAB) micellar solution and CTAB reversed microemulsion by ESR and 2H NMR. *Colloids Surfaces A Physicochem Eng. Asp.* 127 (1–3), 89–96. doi:10.1016/s0927-7757(96)03889-7

Lohse, S. E., and Murphy, C. J. (2013). The quest for shape control: a history of gold nanorod synthesis. *Chem. Mater* 25 (8), 1250–1261. doi:10.1021/cm303708p

Lu, G., Forbes, T. Z., and Haes, A. J. (2016). SERS detection of uranyl using functionalized gold nanostars promoted by nanoparticle shape and size. *Analyst* 141 (17), 5137–5143. doi:10.1039/c6an00891g

Lu, L., Zou, S., and Fang, B. (2021). The critical impacts of ligands on heterogeneous nanocatalysis: a review. *ACS Catal.* 11 (10), 6020–6058. doi:10.1021/acscatal.1c00903

Ma, T., and Liang, F. (2020). Au–Pd nanostars with low Pd content: controllable preparation and remarkable performance in catalysis. *J. Phys. Chem. C* 124 (14), 7812–7822. doi:10.1021/acs.jpcc.0c00031

Magnus, B. L. (2016). Second CMC in surfactant micellar systems. *Curr. Opin. Colloid Interface Sci.* 22, 46–50. doi:10.1016/j.cocis.2016.02.008

Mao, X., Liu, C., Hesari, M., Zou, N., and Chen, P. (2019). Super-resolution imaging of non-fluorescent reactions via competition. *Nat. Chem.* 11 (8), 687–694. doi:10.1038/s41557-019-0288-8

Marbella, L. E., and Millstone, J. E. (2015). NMR techniques for noble metal nanoparticles. *Chem. Mater* 27 (8), 2721–2739. doi:10.1021/cm504809c

Mishra, A., and Das, P. K. (2022). Thermodynamics of multilayer protein adsorption on a gold nanoparticle surface. *Phys. Chem. Chem. Phys.* 24 (37), 22464–22476. doi:10.1039/d2cp02439j

Molina-Bolívar, J. A., Aguiar, J., and Ruiz, C. C. (2002). Growth and hydration of Triton X-100 micelles in monovalent alkali salts: a light scattering study. *J. Phys. Chem. B* 106 (4), 870–877. doi:10.1021/jp0119936

Møller, J. V., and le Maire, M. (1993). Detergent binding as a measure of hydrophobic surface area of integral membrane proteins. *J. Biol. Chem.* 268 (25), 18659–18672. doi:10.1016/s0021-9258(17)46681-6

Mosquera, J., Wang, D., Bals, S., and Liz-Marzán, L. M. (2023). Surfactant layers on gold nanorods. *Acc. Chem. Res.* 56 (10), 1204–1212. doi:10.1021/acs.accounts.3c00101

Narayanan, T. (2009). Synchrotron small-Angle X-ray scattering studies of colloidal suspensions. *Lect. Notes Phys.* 776, 133–156. doi:10.1007/978-3-540-95968-76

Ngo, N. M., Tran, H.-V., and Lee, T. R. (2022). Plasmonic nanostars: systematic review of their synthesis and applications. *ACS Appl. Nano Mater* 5 (10), 14051–14091. doi:10.1021/acsanm.2c02533

Nikoobakht, B., and El-Sayed, M. A. (2003). Preparation and growth mechanism of gold nanorods (NRs) using seed-mediated growth method. *Chem. Mater* 15 (10), 1957–1962. doi:10.1021/cm020732l

Ong, Q., Luo, Z., and Stellacci, F. (2017). Characterization of ligand shell for mixed-ligand coated gold nanoparticles. *Acc. Chem. Res.* 50 (8), 1911–1919. doi:10.1021/acs.accounts.7b00165

Pallavicini, P., Donà, A., Casu, A., Chirico, G., Collini, M., Dacarro, G., et al. (2013). Triton X-100 for three-plasmon gold nanostars with two photothermally active NIR (near IR) and SWIR (short-wavelength IR) channels. *Chem. Commun.* 49 (56), 6265. doi:10.1039/c3cc42999g

Pedrazo-Tardajos, A., Claes, N., Wang, D., Sánchez-Iglesias, A., Nandi, P., Jenkinson, K., et al. (2024). Direct visualization of ligands on gold nanoparticles in a liquid environment. *Nat. Chem.* 16 (8), 1278–1285. doi:10.1038/s41557-024-01574-1

Perinelli, D. R., Cespi, M., Lorusso, N., Palmieri, G. F., Bonacucina, G., and Blasi, P. (2020). Surfactant self-assembling and critical micelle concentration: one approach fits all? *Langmuir* 36 (21), 5745–5753. doi:10.1021/acs.langmuir.0c00420

Peter, C., and Kremer, K. (2009). Multiscale simulation of soft matter systems – from the atomistic to the coarse-grained level and back. *Soft Matter* 5 (22), 4357. doi:10.1039/b912027k

Phan, C. M., and Nguyen, H. M. (2017). Role of capping agent in wet synthesis of nanoparticles. *J. Phys. Chem. A* 121 (17), 3213–3219. doi:10.1021/acs.jpca.7b02186

Pollard, J. M., Shi, A. J., and Göklen, K. E. (2006). Solubility and partitioning behavior of surfactants and additives used in bioprocesses. *J. Chem. Eng. Data* 51 (1), 230–236. doi:10.1021/je0503498

Prévost, S., and Gradzielski, M. (2009). SANS investigation of the microstructures in catanionic mixtures of SDS/DTAC and the effect of various added salts. *J. Colloid Interface Sci.* 337 (2), 472–484. doi:10.1016/j.jcis.2009.05.039

Prozeller, D., Morsbach, S., and Landfester, K. (2019). Isothermal titration calorimetry as a complementary method for investigating nanoparticle-protein interactions. *Nanoscale.* 11 (41), 19265–19273. doi:10.1039/c9nr05790k

Pu, H., Dai, H., Zhang, T., Dong, K., Wang, Y., and Deng, Y. (2022). Metal nanoparticles with clean surface: the importance and progress. *Curr. Opin. Electrochem* 32, 100927. doi:10.1016/j.coelec.2021.100927

Rodríguez-Lorenzo, L., Garrido-Maestu, A., Bhunia, A. K., Espiña, B., Prado, M., Diéguez, L., et al. (2019). Gold nanostars for the detection of foodborne pathogens via surface-enhanced Raman scattering combined with microfluidics. *ACS Appl. Nano Mater* 2 (10), 6081–6086. doi:10.1021/acsanm.9b01223

Rosen, M. J. (1989). Surfactants and interfacial phenomena. *Colloids Surfaces* 40, 347. doi:10.1016/0166-6622(89)80030-7

Saadatkhah, N., Carillo Garcia, A., Ackermann, S., Leclerc, P., Latifi, M., Samih, S., et al. (2020). Experimental methods in chemical engineering: thermogravimetric analysis—TGA. *Can. J. Chem. Eng.* 98 (1), 34–43. doi:10.1002/cjce.23673

Sau, T. K., and Rogach, A. L. (2010). Nonspherical noble metal nanoparticles: colloid-chemical synthesis and morphology control. *Adv. Mater* 22 (16), 1781–1804. doi:10.1002/adma.200901271

Senthil Kumar, P., Pastoriza-Santos, I., Rodríguez-González, B., Javier García de Abajo, F., and Liz-Marzán, L. M. (2008). High-yield synthesis and optical response of gold nanostars. *Nanotechnology* 19 (1), 015606. doi:10.1088/0957-4484/19/01/015606

Shi, Y., Luo, H. Q., and Li, N. B. (2011). Determination of the critical premicelle concentration, first critical micelle concentration and second critical micelle concentration of surfactants by resonance Rayleigh scattering method without any probe. *Spectrochim. Acta Part A Mol. Biomol. Spectrosc.* 78 (5), 1403–1407. doi:10.1016/j.saa.2011.01.018

Smith, J. G., and Jain, P. K. (2016). The ligand shell as an energy barrier in surface reactions on transition metal nanoparticles. *J. Am. Chem. Soc.* 138 (21), 6765–6773. doi:10.1021/jacs.6b00179

Song, T., Gao, F., Guo, S., Zhang, Y., Li, S., You, H., et al. (2021). A review of the role and mechanism of surfactants in the morphology control of metal nanoparticles. *Nanoscale* 13 (7), 3895–3910. doi:10.1039/d0nr07339c

Tao, A. R., Habas, S., and Yang, P. (2008). Shape control of colloidal metal nanocrystals. *Small* 4 (3), 310–325. doi:10.1002/smll.200701295

Tedeschi, A. M., Franco, L., Ruzzi, M., Paduano, L., Corvaja, C., and D'Errico, G. (2003). Micellar aggregation of alkyltrimethylammonium bromide surfactants studied by electron paramagnetic resonance of an anionic nitroxide. *Phys. Chem. Chem. Phys.* 5 (19), 4204. doi:10.1039/b305324p

Tiller, G. E., Mueller, T. J., Dockter, M. E., and Struve, W. G. (1984). Hydrogenation of Triton X-100 eliminates its fluorescence and ultraviolet light absorption while preserving its detergent properties. *Anal. Biochem.* 141 (1), 262–266. doi:10.1016/0003-2697(84)90455-x

Tsoulos, T. V., Han, L., Weir, J., Xin, H. L., and Fabris, L. (2017). A closer look at the physical and optical properties of gold nanostars: an experimental and computational study. *Nanoscale* 9 (11), 3766–3773. doi:10.1039/c6nr09091e

Vigderman, L., Manna, P., and Zubarev, E. R. (2012). Quantitative replacement of cetyl trimethylammonium bromide by cationic thiol ligands on the surface of gold nanorods and their extremely large uptake by cancer cells. *Angew. Chem. Int. Ed.* 51 (3), 636–641. doi:10.1002/anie.201107304

Vilain, C., Goettmann, F., Moores, A., Le Floch, P., and Sanchez, C. (2007). Study of metal nanoparticles stabilised by mixed ligand shell: a striking blue shift of the surface-plasmon band evidencing the formation of Janus nanoparticles. *J. Mater Chem.* 17 (33), 3509. doi:10.1039/b706613a

Villarreal, E., Li, G. G., Zhang, Q., Fu, X., and Wang, H. (2017). Nanoscale surface curvature effects on ligand–nanoparticle interactions: a plasmon-enhanced spectroscopic study of thiolated ligand adsorption, desorption, and exchange on gold nanoparticles. *Nano Lett.* 17 (7), 4443–4452. doi:10.1021/acs.nanolett.7b01593

Walker, D. A., Leitsch, E. K., Nap, R. J., Szleifer, I., and Grzybowski, B. A. (2013). Geometric curvature controls the chemical patchiness and self-assembly of nanoparticles. *Nat. Nanotechnol.* 8 (9), 676–681. doi:10.1038/nnano.2013.158

Wang, H., Pu, Y., Shan, B., and Li, M. (2019). Combining experiments and theoretical modeling to interrogate the anisotropic growth and structure–plasmonic property relationships of gold nanostars. *Inorg. Chem.* 58 (18), 12457–12466. doi:10.1021/acs.inorgchem.9b02187

Wen, Y.-H., Li, L., Li, Y.-M., Zhao, T., and Huang, R. (2021). Molecular dynamics simulations of thermally induced surface and shape evolution of concave Au nanocubes: implications for catalysis. *ACS Appl. Nano Mater* 4 (9), 9527–9535. doi:10.1021/acsanm.1c01994

Wu, M., Vartanian, A. M., Chong, G., Pandiakumar, A. K., Hamers, R. J., Hernandez, R., et al. (2019). Solution NMR analysis of ligand environment in quaternary ammonium-terminated self-assembled monolayers on gold nanoparticles: the effect of surface curvature and ligand structure. *J. Am. Chem. Soc.* 141 (10), 4316–4327. doi:10.1021/jacs.8b11445

Xi, Z., Zhang, R., Kiessling, F., Lammers, T., and Pallares, R. M. (2024). Role of surface curvature in gold nanostar properties and applications. *ACS Biomater. Sci. Eng.* 10 (1), 38–50. doi:10.1021/acsbiomaterials.3c00249

Xiao, J., and Qi, L. (2011). Surfactant-assisted, shape-controlled synthesis of gold nanocrystals. *Nanoscale.* 3 (4), 1383. doi:10.1039/c0nr00814a

Yang, T.-H., Ahn, J., Shi, S., and Qin, D. (2021). Understanding the role of poly(vinylpyrrolidone) in stabilizing and capping colloidal silver nanocrystals. *ACS Nano.* 15 (9), 14242–14252. doi:10.1021/acsnano.1c01668

Ye, R., Zhao, M., Mao, X., Wang, Z., Garzón, D. A., Pu, H., et al. (2021). Nanoscale cooperative adsorption for materials control. *Nat. Commun.* 12 (1), 4287. doi:10.1038/s41467-021-24590-y

Yuan, H., Khoury, C. G., Hwang, H., Wilson, C. M., Grant, G. A., and Vo-Dinh, T. (2012). Gold nanostars: surfactant-free synthesis, 3D modelling, and two-photon photoluminescence imaging. *Nanotechnology* 23 (7), 075102. doi:10.1088/0957-4484/23/7/075102

Yue, Y., Wang, J., and Dai, M. (2000). Volumetric and fluorescence studies of aqueous solutions containing n -octylamine, cetyltrimethylammonium bromide, and salt. *Langmuir* 16 (15), 6114–6117. doi:10.1021/la991530f

Yuk, J. M., Park, J., Ercius, P., Kim, K., Hellebusch, D. J., Crommie, M. F., et al. (2012). High-resolution EM of colloidal nanocrystal growth using graphene liquid cells. *Science* 336 (6077), 61–64. doi:10.1126/science.1217654

Zheng, J., Cheng, X., Zhang, H., Bai, X., Ai, R., Shao, L., et al. (2021). Gold nanorods: the most versatile plasmonic nanoparticles. *Chem. Rev.* 121 (21), 13342–13453. doi:10.1021/acs.chemrev.1c00422

Zhou, H., Jia, H., Zhang, A., Zhang, L., Jia, C., and Zheng, L. (2015). The interconversion between gold nanostars and gold nanodendrites controlled via temperature and the concentration of sodium dodecyl sulfonate. *J. Mol. Liq.* 208, 27–33. doi:10.1016/j.molliq.2015.04.028